Polymer Chemistry

ROYAL SOCIETY OF CHEMISTRY

PAPER

View Article Online
View Journal | View Issue

Cite this: *Polym. Chem.*, 2023, **14**, 477

An unexpected discovery of a one-pot synthesis for carbazole-based diamine and the electrochromic properties of the derived polymers†

Yu-Jen Shao,‡ Yun-Chi Wang‡ and Guey-Sheng Liou *

Unexpected carbazole-based diamine monomers with a hydroxyl group (**E-Cz**) or carbonyl group (**K-Cz**) were successfully synthesized *via* the hydrogenation reaction of **TPA-OBz** in one pot, wherein three different kinds of reactions could happen simultaneously, the reduction of the nitro group, the de-protection of the benzyl group, and the coupling reaction of triphenylamine (TPA). The TPA structure thoroughly transforms into two different carbazole structures depending on the hydrogen source, as characterized by IR, NMR, and HRMS analyses. In addition, three related triarylamine-based polyamides (**TPA-PA**, **E-Cz-PA**, and **co-OH-PA**) were also prepared to investigate their electrochromic (EC) performance. The hydroxyl groups of **E-Cz** provide active sites for the *in situ* sol–gel reaction with the metal oxide precursor to form hybrid films. The resulting polyamide hybrid films showed effectively improved EC behaviors during the redox process by accelerating the charge transfer due to the donor–acceptor system. Consequently, the polyamide hybrid films possess a lower driving potential, more negligible charge transfer resistance (R_{ct}), and shorter switching and bleaching response times. The hybrid film (**co-Zr20-PA**) could be further fabricated into an electrochromic device (ECD) and it demonstrated highly stable switching reversibility over one hundred cyclic switches.

Received 8th August 2022,
Accepted 21st December 2022

DOI: 10.1039/d2py01030e

rsc.li/polymers

Introduction

Arylamines are well-known for their excellent hole-transporting mobility, electron-rich characteristics, and electrochemical stability.[1] Due to the electron-donating nature of the nitrogen atom, arylamine derivatives can be applied in light-emitting diodes, solar cells, photovoltaics, and electrochromic materials.[2–4] In addition, arylamine derivatives are easily oxidized to form radical cations, resulting in color changes in the visible region. Consequently, arylamine-based polymers have become promising materials for electrochromic (EC) applications.[5] Among these arylamine structures, carbazoles are widely used in research, as they are easily functionalized at the 3,6- and 2,7-positions.[6–8] Generally, the preparation of carbazoles involves Borsche–Drechsel cyclization, Graebe–Ullman reaction, and Nitrene insertion.[9–11] They can also be synthesized *via* coupling reaction using metal catalysts to form the C–C or C–N bond,[12,13] and N-substituted carbazole can be prepared with various groups to form versatile *N*-phenylcarbazoles (NPCs) to tune the optical and electrical properties.[14–19] Knölker's group reported a palladium-catalyzed method to prepare various carbazoles from arylamines.[20–22] The presence of palladium(II) in the reaction leads to the formation of the central C–C bond of the carbazole and palladium(II) changes to palladium(0). Typically, this palladium-catalyzed method needs an oxidant to reoxidize the palladium(0) like the copper(II) salt, fulfilling the catalytic cycle for the coupling process from *N*,*N*-diarylamines to carbazoles, known as the Åkermark–Knölker cyclization reaction.

As previously mentioned, carbazole-based materials are also attractive candidates in the field of electrochromism. A good EC material should possess the following characteristics: a low driving potential, short response time, high color contrast, and redox reversibility.[23] To promote the EC performance, our group has attempted to introduce hydroxyl groups or carboxylic groups into polymer chains to hybridize with metal oxides (*e.g.*, TiO_2 and ZrO_2) by covalent bonds *via in situ* sol–gel reaction to increase the charge transfer capability of the polymer film, as described in previous reports.[24,25] During the redox process, the metal oxide can act as an electron storage center to transfer electrons back and forth through the hybrid film owing to the donor-accepter system, which enhances the switching and bleaching response behaviors.[26] Furthermore, introducing heptyl viologen (HV) into electrochromic devices

Institute of Polymer Science and Engineering, National Taiwan University, Taipei 10617, Taiwan. E-mail: gsliou@ntu.edu.tw

†Electronic supplementary information (ESI) available: Measurements, ^{1}H-NMR, COSY, HSQC, and HRMS. See DOI: https://doi.org/10.1039/d2py01030e

‡These authors equally contributed to this work.

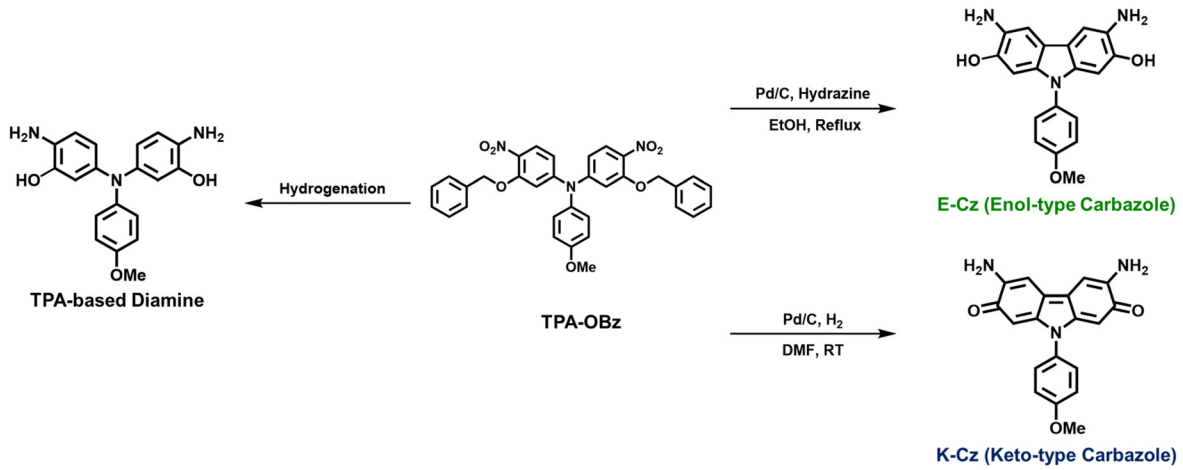

Scheme 1 The synthetic route of the unexpected carbazole-type products in this study.

(ECDs) as a counter EC layer for charge balance helps to reduce the driving potential and response time and strengthen other properties.[27]

In this study, we discovered a new route that can transform the triphenylamine (TPA) intermediate (**TPA-OBz**) into two carbazole diamine structures (**E-Cz** and **K-Cz**) using palladium on active carbon (Pd/C) with different hydrogen sources (Scheme 1), demonstrating that the reduction of nitro groups, deprotection of hydroxyl groups, and metal-induced coupling reaction happen simultaneously. To investigate the electrochemical and EC properties, **E-Cz** was further used to prepare a homopolymer (**E-Cz-PA**) and copolymers (**co-OH-PA**) *via* low-temperature polymerization because the hydroxyl groups substituted on the carbazole ring act as the active sites for *in situ* sol–gel reaction. The EC properties of the resulting polymers and the corresponding hybrid films were measured and investigated, using spectroelectrochemistry and EC switching studies, by casting onto ITO glass. In addition, the **co-Zr20-PA** hybrid film was also prepared to fabricate into an ECD with HV. The color of the ECD changed from almost colorless to nearly truly black during the switching-on process because of the panchromatic broad absorption peak over the visible-light region, which is also a synergetic effect of the copolymer material.

Experimental section

Materials

4,4′-Diamino-4″-methoxytriphenylamine (TPA-OMe) was prepared according to a previous method. Other commercially available materials, such as *N*,*N*-dimethylacetamide (DMAc) (TEDIA), *N*-methyl-2-pyrrolidone (NMP) (MACRON), pyridine (Py) (ACROS), triphenyl phosphite (TPP) (ACROS), adipic acid (SHOWA), adipoyl chloride (Alfa Aesar), calcium chloride (ACROS), and zirconium(IV) butoxide ($Zr(OBu)_4$) solution (TCI), were used without purification. The electrolyte, tetrabutylammonium tetrafluoroborate ($TBABF_4$), for electro-chemical measurement was prepared by the following steps. Saturated tetrafluoroborate ($NaBF_4$) (ACROS) was mixed with drops of a tetrabutylammonium bromide (TBABr) (TCI) aqueous solution. Then, the white precipitate was purified using ethanol and water. Heptyl viologen di-tetrafluoroborate ($HV(BF_4)_2$), abbreviated as HV, was prepared by the following steps. Heptyl viologen dibromide ($HVBr_2$) was prepared by mixing 4,4′-bipyridine (Alfa Aesar) and 1-bromoheptane (Alfa Aesar) in acetonitrile. Then, the yellow precipitation was washed with chloroform, dissolved in DI water, and dropped into a saturated $NaBF_4$ aqueous solution. Finally, the white precipitate was recrystallized using ethanol.

Synthesis of 3,3′-di(benzyloxy)-4″-methoxy-4,4′-dinitrotriphenylamine (TPA-OBz)

p-Anisidine (2.5 g, 10 mmol) (1), 2-benzyloxy-4-fluoronitro benzene (2.8 g, 20 mmol) (2), and dried cesium fluoride (3 g, 20 mmol) were added to dimethyl sulfoxide (40 mL) in a 100 mL three-neck flask. The solution was stirred at 100 °C for 3 days and then extracted with water and ethyl acetate. The organic layer was dried with magnesium sulfate and rotary evaporation. The red crystals were recrystallized using a condensed ethyl acetate solution and methanol. The red crystals (4 g, yield 69%) were collected by filtration and dried in a vacuum oven. Mp: 145–147 °C measured by DSC at 10 °C min^{-1}. The FT-IR spectrum (KBr) shows absorption bands at 2840 (C–H stretching), 1574 and 1300 cm^{-1} (symmetric and asymmetric N=O stretching). ^{1}H NMR (600 MHz, DMSO-*d*6, *δ*, ppm): 3.82 (s, 3H, H_j), 5.13 (s, 4H, H_d), 6.57 (d, 2H, H_b), 6.88 (s, 2H, H_c), 7.01 (d, 2H, H_i), 7.15 (d, 2H, H_h), 7.34 (m,10H, H_{e+f+g}), 7.90 (d, 2H, H_a). ^{13}C NMR (150 MHz, DMSO-d_6, *δ*, ppm): 55.36 (C_{16}), 70.39 (C_7), 107.91 (C_5), 113.76 (C_3), 115.57 (C_{14}), 127.10 (C_9), 127.53 (C_2), 127.88 (C_{11}), 128.39 (C_{10}), 128.90 (C_{13}), 133.46 (C_1), 135.77 (C_8), 136.57 (C_{12}), 151.41 (C_4), 153.24 (C_6), 157.94 (C_{15}). Anal. calcd for $C_{33}H_{27}N_3O_7$: C, 68.62%; H, 4.71%; N, 7.28%. Found: C, 68.84%; H, 4.66%; N, 7.36%. HRMS (*m*/*z*), [M + H^+] calculated: 578.1922, found: 578.1918.

Synthesis of *N*-(4-methoxy)-2,7-dihydroxy-3,6-diamino-9*H*-carbazole (E-Cz)

TPA-OBz (4 g, 7.04 mmol) was added to ethanol (40 mL) in a 100 mL three-neck flask. Then, Pd/C (10%, 400 mg) and hydrazine monohydrate were added under nitrogen flow. The system was refluxed for one day. The solution was filtered through a Celite pad to remove Pd/C. Blue needle crystals could be obtained after cooling the filtrate to room temperature. The product (1.0 g, yield 42%) was collected by filtration and dried under a vacuum. Mp: 206–209 °C measured by DSC at 10 °C min^{-1}. The FT-IR spectrum (KBr) shows absorption bands at 3500–3100 cm^{-1} (O–H and N–H stretching). ^{1}H NMR (600 MHz, DMSO-d_6, δ, ppm): 3.84 (s, 3H, H_e), 4.24 (s, 4H, $-NH_2$), 6.62 (s, 2H, H_b), 7.05 (s, 2H, H_a), 7.15 (d, 2H, H_d), 7.38 (d, 2H, H_c). ^{13}C NMR (150 MHz, DMSO-d_6, δ, ppm): 55.40 (C_{11}), 93.37 (C_5), 103.73 (C_2), 114.96 (C_9), 115.32 (C_3), 127.20 (C_8), 130.55 (C_1), 131.33 (C_7), 133.65 (C_4), 143.40 (C_6), 157.40 (C_{10}). HRMS (*m*/*z*), [M + H^+] calculated: 336.1343, found: 336.1340.

Synthesis of *N*-(4-methoxyphenyl)-3,6-diaminocarbazole-2,7-dione (K-Cz)

TPA-OBz (1 g, 1.76 mmol) was added to DMF (20 mL) in a 100 mL three-neck flask with Pd/C (10%, 100 mg). The mixture was vigorously stirred under a hydrogen atmosphere at room temperature for three days. The solution was filtered through a Celite pad to remove Pd/C and then precipitated into water drop by drop to yield dark-blue crystals (0.5 g, yield 86%), which were collected by filtration and dried under vacuum. The melting point is unavailable due to decomposition before 150 °C (investigated by TGA with a heating rate of 10 °C min^{-1} under a nitrogen atmosphere, as shown in Fig. S1†). The FT-IR spectrum (KBr) shows absorption bands at 3400–3200 cm^{-1} (N–H stretching) and 1620 cm^{-1} (C=O stretching). ^{1}H NMR (600 MHz, DMSO-d_6, δ, ppm): 3.81 (s, 3H, H_e), 5.10 (s, 2H, H_a), 5.84 (s, 2H, H_b), 6.03 (s, 4H, $-NH_2$), 7.07 (d, 2H, H_d), 7.30 (d, 2H, H_c). ^{13}C NMR (150 MHz, DMSO-d_6, δ, ppm): 55.87 (C_{11}), 94.46 (C_5), 101.06 (C_2), 115.60 (C_9), 127.17 (C_1), 127.24 (C_3), 128.31 (C_8), 141.80 (C_7), 157.39 (C_4), 159.03 (C_{10}), 181.99 (C_6). HRMS (*m*/*z*), [M + H^+] calculated: 334.1186, found: 334.1182.

Synthesis of TPA-PA

0.29 g (2 mmol) of adipic acid was added into 3.6 mL of NMP (20 wt%) with 0.24 g of $CaCl_2$, 1 mL of pyridine, and 1.4 mL of TPP. Then, **TPA-OMe** (2 mmol) was added to the solution (Scheme 2a). The mixture was heated up to 110 °C and kept there for 4 hours. The solution was poured into methanol/water (1 : 1, v/v) after cooling to room temperature. A fiber-like precipitation was obtained, which was purified by Soxhlet extraction with methanol for 2 days, and dried under vacuum at 100 °C.

Synthesis of E-Cz-PA

0.68 g (2 mmol) of **E-Cz** was first added into a flask with 4 mL of NMP (20 wt%). The solution was frozen under liquid nitrogen, then 0.37 g (2 mmol) of adipoyl dichloride was added to the flask. As the surface of the mixture started melting, 0.34 mL of propylene oxide was added (Scheme 2a). The solution slowly reacted from −20 °C to room temperature for 6 hours. The polymer was precipitated using methanol/water (1 : 1, v/v), purified by Soxhlet extraction with methanol for 2 days, and dried under a vacuum at 100 °C.

Synthesis of co-OH-PA

0.34 g (1 mmol) of **E-Cz** and 0.31 g of **TPA-OMe** (1 mmol) were first added into a flask with 4 mL of NMP (20 wt%). The solution was frozen under liquid nitrogen, then 0.37 g (2 mmol) of adipoyl dichloride was added to the mixture (Scheme 2a). The subsequent procedure was the same as that for **E-Cz-PA** mentioned above.

Preparation of co-OH-PA/zirconia hybrid films (co-Zr-PA)

30 mg of **co-OH-PA** was dissolved in 10 mL of DMAc with 0.1 mL of acetic acid added slowly under vigorous stirring for

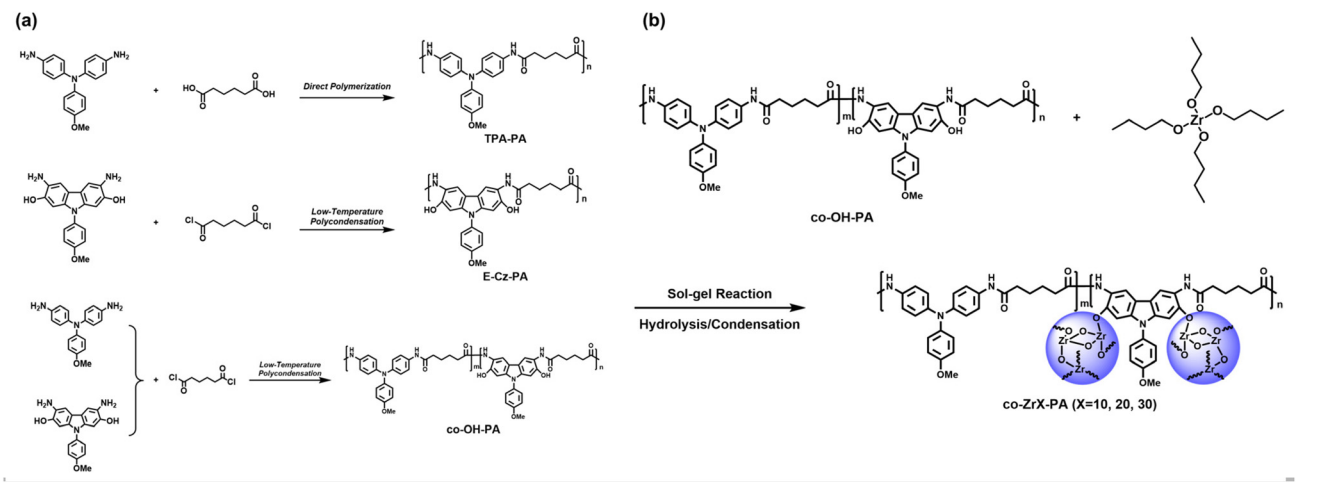

Scheme 2 Preparation of (a) the resulting polyamides and (b) the hybrid films of the copolymer.

1 hour; another solution of 1 : 1 $Zr(OBu)_4$/butanol was added into the polymer solution drop by drop and stirred for 10 minutes (Scheme 2b). Different amounts of ZrO_2 were added, and co-ZrXPA (X = 10, 20, and 30) represents the weight percentage of ZrO_2 in the hybrid films. The solution was filtrated through 0.22 μm PTFE filters, drop coated onto ITO glass, and dried in a vacuum at room temperature for 5 hours, 80 °C for 2 hours, 160 °C for 2 hours, and 200 °C for 8 hours. TGA was also utilized to identify the content of the inorganic species in the hybrid films, as shown in Fig. S2.†

Results and discussion

Synthesis and primary characterization of the monomers

TPA-OBz was synthesized from *p*-anisidine and 2-benzyloxy-4-fluoronitrobenzene by nucleophilic substitution reaction (Fig. S3–S5†). **E-Cz** and **K-Cz** were prepared by using the Pd/C catalyst with different hydrogen sources: hydrazine monohydrate and hydrogen, respectively. The synthetic routes of the three monomers are summarized in Scheme 1. According to a previous study, our group initially intended to synthesize a TPA-type diamine with hydroxyl groups instead of the carbazole one.[28] However, we unexpectedly discovered that a different reaction occurs during the hydrogenation, transforming the resulting TPA-based product into a carbazole. Consequently, we designed and conducted two experiments to investigate the structure of the final products. The most exciting thing is that these two experiments came out with different structures. Firstly, the final product of the hydrogenation of **TPA-OBz** with hydrazine monohydrate as the hydrogen source and EtOH as the solvent was an enol-type carbazole-diamine (**E-Cz**), carefully characterized using IR, NMR, and high-resolution electrospray ionization mass spectrometry (HRMS). Absorption peaks of amino ($-NH_2$) and hydroxyl (–OH) groups appear in the IR spectrum in the range of 3100–3500 cm^{-1} (Fig. 1a). The ^{1}H-NMR spectrum revealed that there are eight protons (carbazole structure) in the aromatic region instead of ten protons (expected TPA structure) (Fig. 1b). Moreover, the 13C-NMR and DEPT analyses demonstrated that the **E-Cz** product has six different quaternary carbon atoms in the aromatic region instead of five (Fig. S6, S7, and S8a†), and the HRMS results also indicated that the exact mass is 336.1340 (Fig. S9†). Therefore, we could confirm that the TPA derivative was transformed into the carbazole derivative. As a result, we speculated that the hydrogenation of **TPA-OBz** simultaneously included three reactions during the process: the reduction of the nitro group, the deprotection of the benzyl group, and the metal-induced coupling reaction. Some studies have reported that the *N*,*N*-diphenylamine moiety can undergo coupling reaction to form the carbazole moiety in the presence of Pd(II) as an oxidative agent.[20] In this work, because the Pd(II)-intermediate product is generated from deprotection of the benzyl group of **TPA-OBz**, the Pd(II)-intermediate product might react with the electron-rich C–H bond at the 2 and 2′ positions to enable the Åkermark–Knölker reaction to transform the central C–C bond, forming the carbazole moiety, and the proposed reaction route is illustrated in Schemes S1 and S2.†[29]

This phenomenon also occurred in the following reaction under a hydrogen atmosphere at room temperature for three days. The final product under this condition was a keto-type carbazole-diamine (**K-Cz**), also characterized using IR, NMR, and HRMS. The absorption peak of $-NH_2$ stretching appears

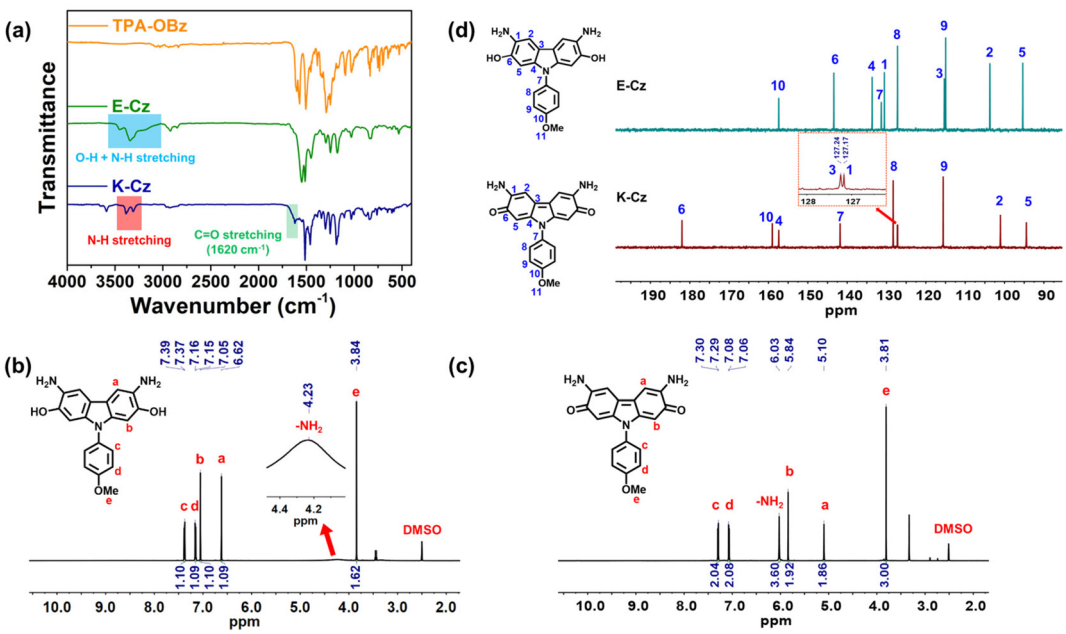

Fig. 1 (a) FT-IR spectra of the monomers. ^{1}H-NMR spectra of (b) **E-Cz** and (c) **K-Cz** in DMSO-d_6. (d) Comparison of ^{13}C-NMR spectra of (up) **E-Cz** and (down) **K-Cz** in DMSO-d_6.

in the IR spectra, with a new absorption peak of carbonyl groups located at 1620 cm^{-1} (Fig. 1a). Unlike the regular C=O stretching, the absorption peak of the carbonyl group shows a bathochromic shift due to the effect of the hydrogen bond, the hyperconjugation of enone, and the ring strain. By comparing the ^{13}C-NMR spectra of **K-Cz** and **E-Cz** shown in Fig. 1d, it is clear that the formed carbonyl group caused the C_6 in **K-Cz** to shift the most downfield to 181.99 ppm, and C_1 shifted upfield due to the destruction of the aromatic system in the carbazole unit, reducing the deshielding effect. Furthermore, the ^{13}C NMR and DEPT analyses of **K-Cz** revealed six different quaternary carbon atoms, indicating the formation of a carbazole-based structure, as shown in Fig. S8b, S10, and S11.† The ^{1}H-NMR spectrum showed that the protons H_a and H_b (5.10 and 5.84 ppm) shift to upfield in comparison with **E-Cz** (7.05 and 6.62 ppm), implying that the aromatic system is destroyed on the carbazole ring (Fig. 1c). Typically, the temperature of the Åkermark–Knölker reaction for diphenylamine coupling to yield a product with an aromatic carbazole structure should be higher.[12,13] However, the reaction temperature of **K-Cz** was room temperature in DMF, implying another reaction pathway to form the keto-type product with a non-aromatic carbazole structure, which is different from the typical Åkermark–Knölker reaction, although the coupling reaction still occurs. Besides, the resonance signal at 6.03 ppm could be assigned to the amino protons according to the ^{13}C–^{1}H HSQC spectrum (Fig. S11b†). The downfield shifting and sharpened intensity of amino protons could be attributed to the stronger hydrogen bonding and less deuterium exchange effect between the amino and carbonyl groups than for **E-Cz**. Furthermore, the HRMS result also showed that the exact mass is 334.1182 (Fig. S12†), which is two fewer protons than **E-Cz**. Combining the IR, NMR, and HRMS results, we could confirm that this final product is a non-aromatic carbazole-based monomer with carbonyl groups (**K-Cz**). The electrochemical and spectroelectrochemical behaviours were also investigated using OTTLE, as shown in Fig. S13.† **E-Cz** (1.65 V) showed a lower oxidation potential than **K-Cz** (1.96 V) due to its higher conjugation in the aromatic plane. In addition, in the spectroelectrochemical spectra, compared to **K-Cz**, **E-Cz** revealed a more red-shifted absorption at 579 nm after applying the oxidation potential, confirming the longer conjugation length across the whole structure.

Synthesis of the resulting polymers and their basic properties

E-Cz was used to prepare EC polymer materials for investigating the electrochemical and EC behaviours, due to the aromatic system and the hydroxyl groups. In addition, the resulting polyamides could undergo *in situ* sol–gel reaction with hydroxyl groups as active sites to enhance the EC performance. As shown in Scheme 2a, three polyamides (**TPA-PA**, **E-Cz-PA**, and **co-OH-PA**) were synthesized from two different diamines (**TPA-OMe** and **E-Cz**) and adipoyl dichloride, and their inherent viscosities, molecular weights, and solubility are summarized in Tables S1 and S2.† Besides, the *in situ* sol–gel reaction of **co-ZrX-PA** (X = 10, 20, and 30) is illustrated in Scheme 2b. The thermal properties of **TPA-PA**, **E-Cz-PA**, and **co-OH-PA** were measured using TGA and DSC (Fig. S14†), and they are summarized in Table S3.† According to the results, the hydroxyl-containing polyamides, **E-Cz-PA** and **co-OH-PA**, exhibited two-stage degradation in the nitrogen atmosphere. During the cyclodehydration at around 250 °C, the hydroxyl groups in the polyamide react with the amide linkage to release two H_2O molecules per repeat unit and transform into polybenzoxazole. Experimentally, the weight loss of **E-Cz-PA** was 7.7 wt%, and the weight loss of **co-OH-PA** was 4.3 wt% after cyclodehydration, corresponding to the theoretical values (**E-Cz-PA:** 7.5 wt% and **co-OH-PA:** 4.0 wt%). In addition, **E-Cz-PA** exhibited the highest T_g at 215 °C, while **co-OH-PA** had the lowest (140 °C), implying that the packing between the copolymer chains was suppressed.

Electrochromic properties of polyamide films

Optical and electrochemical properties

The transmittance of the prepared polyamide films coated on ITO glass measured by UV-vis spectroscopy is shown in Fig. S15,† confirming that they possessed high transparency over the visible light region, even the hybrid films with ZrO_2 contents up to 30 wt%. The electrochemical characteristics of these films were studied using cyclic voltammetry (CV), as shown in Fig. 2 and S16.† As can be seen in Fig. 2, the driving potential of **E-Cz-PA** was higher than that of **TPA-PA**, resulting from the electron-withdrawing ability of the hydroxyl group at the *meta* position. However, the corresponding reduction peak of **E-Cz-PA** did not appear in the CV diagram, indicating that

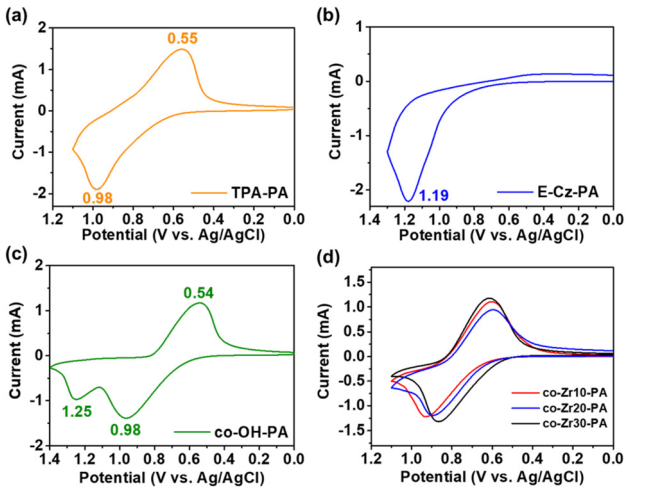

Fig. 2 CV diagrams of (a) **TPA-PA** film (thickness: 180 ± 20 nm), (b) **E-Cz-PA** film (thickness: 200 ± 30 nm), (c) **co-OH-PA** film (thickness: 210 ± 20 nm), and (d) **co-ZrX-PA** (X = 10, 20, 30) hybrid films (thickness: **co-Zr10-PA**: 220 ± 20 nm, **co-Zr20-PA**: 240 ± 30 nm and **co-Zr30-PA**: 270 ± 40 nm) on the ITO-coated glass substrate (coated area: 0.6 cm × 3 cm) in 0.1 M $TBABF_4$/MeCN at a scan rate of 50 mV s^{-1}.

the lone pairs of the nitrogen atoms prefer to localize with the coplanar ring of carbazole rather than the twisted TPA.[17,30] Besides, **co-OH-PA** revealed two oxidation peaks with the higher one (1.25 V) related to **E-Cz-PA** and the lower one (0.98 V) related to **TPA-PA**, respectively. Furthermore, the **E-Cz** moiety in **co-OH-PA** provides the active sites for generating ZrO_2 nanoparticles as electron-storage units, which accept and return electrons transferred from the oxidized nitrogen atom *via* covalent bonds to shorten the switching response time efficiently. The results showed that **co-Z10-PA** has a lower oxidation potential (0.93 V) than **TPA-PA** (0.98 V), whereas **co-Zr20-PA** and **co-Zr30-PA** could further lower the driving potentials. Furthermore, among all the polyamide films, the corresponding reduction peak and the potential difference between oxidation and reduction peaks (ΔE) of **co-Zr30-PA** were the highest (0.62 V) and the lowest (0.24 V), respectively, implying that **co-Zr30-PA** has the best response behaviour, as reported in the following section. Specifically, the electrochemical performance of **co-Zr-PA** was enhanced significantly as the amount of ZrO_2 increased, which means that the hybrid film improves the electrochemical behaviour, and the results are summarized in Table 1.

Spectroelectrochemistry

The EC polyamide films were deposited on ITO glass to investigate the optical characteristics using spectroelectrochemical tests. Fig. 3 shows the spectroelectrochemical spectra of **TPA-PA**, **E-Cz-PA**, and **co-OH-PA** films with varied applied potentials. The **TPA-PA** and **co-OH-PA** films appeared colourless in the neutral state (0 V), whereas the **E-Cz-PA** film was yellowish. The intensity of absorption peaks at 380 and 785 nm for **TPA-PA** increased with increasing applied driving potential after oxidation, attributed to the TPA unit forming a stable monocation radical. As a result, the colour of the **TPA-PA** film changed from colourless to blue. During the oxidation of **E-Cz-PA**, the characteristic peaks of 387, 456, and 950 nm gradually increased in intensity, resulting from formation of the stable monocation radical of the carbazole moiety, which causes the colour of the **E-Cz-PA** film to become a darker yellow. The spectroelectrochemical spectra of **co-OH-PA** revealed a combination

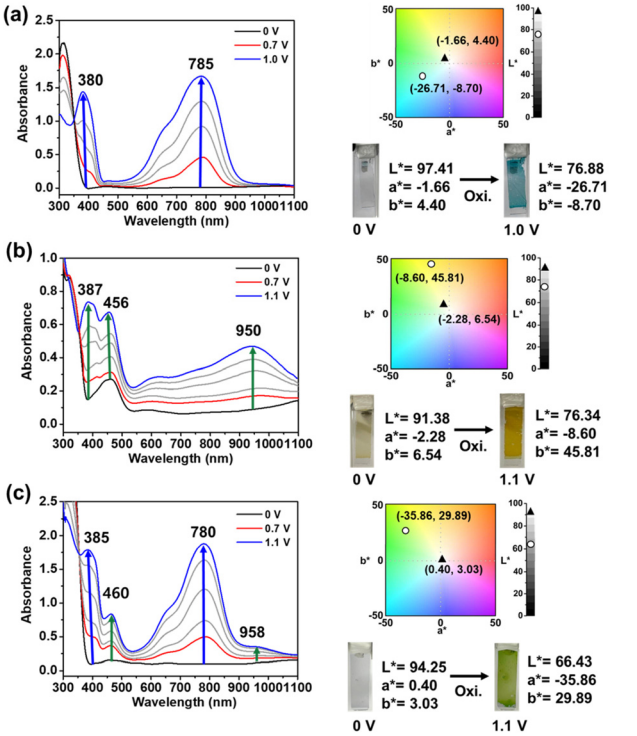

Fig. 3 Spectroelectrochemical spectra and CIELAB color space of (a) **TPA-PA** (thickness: 180 ± 20 nm), (b) **E-Cz-PA** (thickness: 200 ± 30 nm), and (c) **co-OH-PA** (thickness: 350 ± 40 nm) measured on the ITO-coated glass substrate in 0.1 M $TBABF_4$/MeCN.

Table 1 Redox peak potentials of all prepared films

Polyamides	E_{ox} [a] (V)	δE_{ox} [b] (V)	E_{red} [c] (V)	δE_{red} [d] (V)	ΔE [e] (V)	$\delta \Delta E$ [f] (V)
TPA-PA	0.98	—	0.55	—	0.43	—
co-OH-PA	0.98	0.00	0.54	−0.01	0.44	−0.01
co-Zr10-PA	0.93	0.05	0.60	0.05	0.33	0.10
co-Zr20-PA	0.89	0.09	0.60	0.05	0.29	0.12
co-Zr30-PA	0.86	0.13	0.62	0.07	0.24	0.21

[a] Oxidation potential at the peak. [b] The difference in oxidation potentials between the selected polymer and **TPA-PA** films. [c] Reduction potential at the peak. [d] The difference in reduction potentials between the chosen polymer and **TPA-PA** films. [e] Potential difference between oxidation and reduction peaks, $|E_{ox} - E_{red}|$. [f] The difference of potential difference between the specified polymer and **TPA-PA** films.

of emerging characteristic peaks of **TPA-PA** and **E-Cz-PA** during the oxidation, where the peaks at 385 and 768 nm were related to the TPA monocation radical in **TPA-PA** and the peaks at 468 and 950 nm were related to the monocation radical of carbazole in **E-Cz-PA**, respectively. Consequently, the **co-OH-PA** film exhibited a dense green colour after oxidation.

Electrochromic switching properties

The EC switching response was studied at a selected wavelength during the redox process of the corresponding polyamide films in the states of oxidation and reduction, each for 50 seconds. The colouring and bleaching times of the films were calculated by the transmittance change at the specific wavelength as a function of time, as illustrated in Fig. S16.† The colouring time indicates when the EC films reached 90% of total transmittance change from bleaching state to colouring state and *vice versa*. The colouring and the bleaching voltages were set as 1.0 V and 0.0 V, respectively, to ensure the polymer films were fully oxidized and reduced based on Fig. 2. Fig. S17† shows that **co-OH-PA** had the longest colouring and bleaching times of 4.4 s and 12.4 s, respectively, whereas **TPA-PA** revealed a colouring time (t_c) of 4.2 s and a bleaching time (t_b) of 9.0 s. The hybrid films of **co-Zr10PA** (t_c: 3.8 s, t_b: 2.7 s), **co-Zr20PA** (t_c: 2.7 s, t_b: 2.0 s), and **co-Zr30PA** (t_c: 2.4 s, t_b: 2.4 s) exhibited progressively decreasing colouring and bleaching times due to the presence of ZrO_2 serving as electron-

storage sites to enhance the speed of charge transportation. Namely, the more ZrO_2 added to the polymer film, the better the switching response capabilities of the polymer film. Moreover, the coloration efficiency (η) and optical density (ΔOD) of the obtained polymer films were also calculated and are tabulated in Table S4.† The results demonstrate that the current consumption decreased with increasing content of ZrO_2 in the hybrid films, evidencing that ZrO_2 nanoparticles facilitate the charge transfer during the redox process as an electron-storage unit and could further enhance the coloration efficiency. Therefore, the current consumption and the colouration efficiency of **co-Zr30-PA** were the smallest and highest, respectively.

Electrochemical impedance spectroscopy

Electrochemical impedance spectroscopy (EIS) is a technique for demonstrating the mass and charge transfer resistance of electrodes in electrochemical experiments by perturbing the cell with small amplitudes and obtaining a linear current–potential response that can be fit with an equivalent circuit. Fig. 4 shows the Nyquist plots of the resulting films, obtained by using a Randles circuit with a solution resistance (R_Ω) in series with a parallel connection of a charge transfer resistance (R_{ct}) and Warburg resistance (Z_w) and a double-layer capacitance (C_{dl}). The diameter of the semi-circle at high frequency was used to fit and calculate the R_{ct} values of the polymer films. According to the results, the **co-Zr30-PA** film had the lowest R_{ct} value of 39.76 Ω, while the **co-OH-PA** film had the highest R_{ct} value of 54.49 Ω. Furthermore, with increasing content of ZrO_2 in the hybrid films, the R_{ct} value of the hybrid films decreased from 44.58 Ω to 39.76 Ω. Consequently, incorporating ZrO_2 into the polymer improves the charge transfer capability, resulting in an efficient switching response.

Electrochromic properties of ECDs

For further application, two prepared polymers, **TPA-PA** and **co-Zr20-PA**, were fabricated into electrochromic devices (ECDs) in the following studies to investigate the effect of the hybrid film containing ZrO_2. The ECDs were injected with an electrolyte solution containing 165 mg (0.1 M) of $TBABF_4$ and 40 mg (15 μM) of HV in 5 mL of propylene carbonate (PC). According to a previous study, ECDs are more stable in the presence of HV since HV^{2+} accepts electrons from TPA during oxidation and transforms into HV^{+} to reduce the applied voltage window.[27,31,32] Therefore, ECDs with HV could have lower oxidation potentials and shortened switching response times. The oxidation potential of **ECD-*co*-Zr20-PA** was 1.21 V, whereas that of **ECD-TPA-PA** and **ECD-*co*-OH-PA** was 1.30 V and 1.33, respectively, as shown in Fig. S18 and Table S5.† Furthermore, **ECD-*co*-Zr20-PA** exhibited a slightly higher reduction potential than **ECD-TPA-PA** and **ECD-*co*-OH-PA**. To summarize, the ΔE of **ECD-*co*-Zr20-PA** (0.19 V) with the help of ZrO_2 was substantially lower than that of **ECD-TPA-PA** (0.29 V) and **ECD-*co*-OH-PA** (0.35 V), indicating that **ECD-*co*-Zr20-PA** manifests a better EC performance. Besides, according to the response time results (Fig. 6a and b), **ECD-*co*-OH-PA** exhibited similar t_c and t_b values to those of **ECD-TPA-PA**. Therefore, the following discussion will focus on the enhanced properties between **ECD-TPA-PA** and **ECD-*co*-Zr20-PA**.

The spectroelectrochemical spectra with various applied potentials of **ECD-TPA-PA** and **ECD-*co*-Zr20-PA** are shown in Fig. 5. The characteristic peaks of HV^{+} that locate at 608 to 615 nm appeared for both ECDs. According to the CIELAB results, the appearance of **ECD-*co*-Zr20-PA** (L^*: 31.93; a^*: −22.50; b^*: −28.07) in the colouring state was much denser than **ECD-TPA-PA** (L^*: 62.30; a^*: −14.05; b^*: −32.66), due to an additional characteristic peak of the carbazole moiety at 458 nm. The applied potentials for colouring and bleaching were set at 1.2 V and −0.3 V, respectively. Moreover, the switching response time at the wavelengths of 760 nm and 766 nm for three ECDs during the redox process is illustrated in Fig. 6a–c. The colouring and bleaching times of **ECD-TPA-PA**

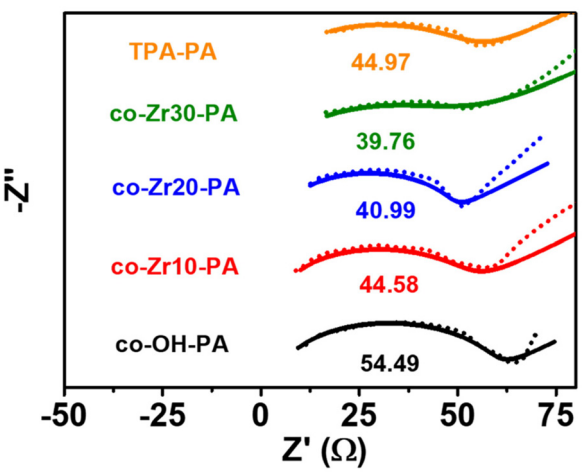

Fig. 4 Nyquist plots of prepared polyamide films in the oxidation state.

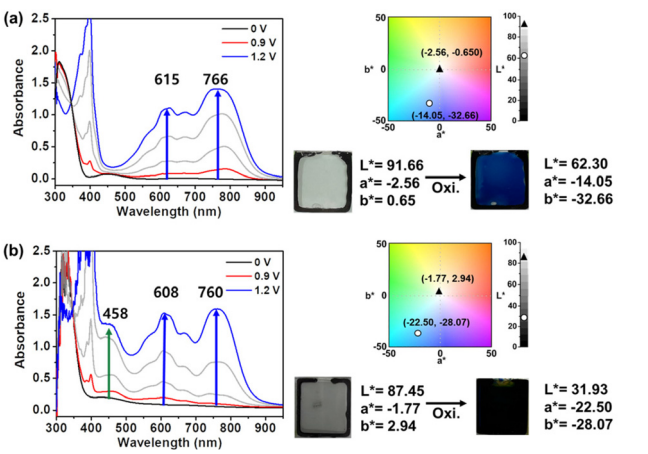

Fig. 5 Spectroelectrochemical spectra of (a) **ECD-TPA-PA** (thickness: 180 ± 20 nm) and (b) **ECD-*co*-Zr20-PA** (thickness: 240 ± 30 nm) measured on the ITO-coated glass substrate with 0.1 M $TBABF_4$ and 15 μM HV in 48 μL of PC.

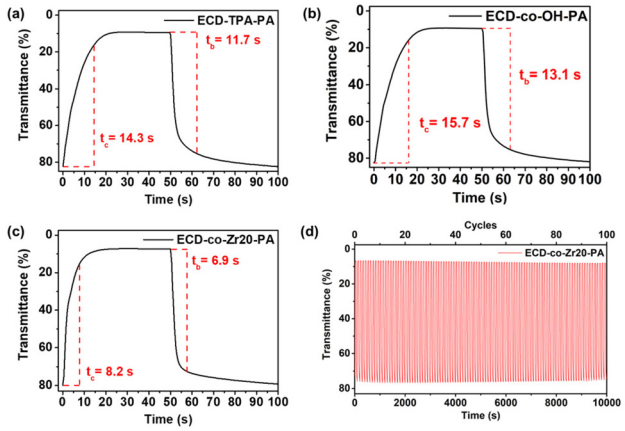

Fig. 6 Switching response time at (a) 766 nm of **ECD-TPA-PA** (thickness: 180 ± 20 nm), (b) 766 nm of **ECD-*co*-OH-PA** (thickness: 200 ± 20 nm), (c) 760 nm of **ECD-*co*-Zr20-PA** (thickness: 240 ± 30 nm) and (d) switching capability at 760 nm of **ECD-*co*-Zr20-PA** for 100 cycles (cycle time: 100 s) on ITO glass (active area: 2 cm × 2 cm) with 1.2 V as the coloring voltage and −0.3 V as the bleaching voltage with 0.1 M $TBABF_4$ and 15 μM HV in 48 μL of PC.

were 14.3 s and 11.7 s, respectively, while those of **ECD-*co*-Zr20-PA** were 8.2 s and 6.9 s, confirming that the device, with the help of ZrO_2, exhibited a faster response capability. Besides, the switching stability of **ECD-*co*-Zr20-PA** was studied with a cycle time of 100 s (colouring time and bleaching time each of 50 s) for 100 cycles, as shown in Fig. 6d and tabulated in Table S6.† The decay of transmittance change after one hundred cycles of colouring and bleaching was only 3.6%, implying that **ECD-*co*-Zr20-PA** has high electrochemical stability.

Conclusions

The unexpected carbazole-based diamines obtained *via* hydrogenation, **E-Cz** and **K-Cz**, were successfully synthesized and investigated. In this unique synthesis route, the hydrogenation of **TPA-OBz** with Pd/C in one pot includes three reactions that happened simultaneously: the reduction of the nitro group, the deprotection of the benzyl group, and the coupling reaction of triphenylamine. It is worth mentioning that different hydrogen sources can produce different final products with aromatic or non-aromatic carbazole structures. Besides, three aromatic polyamides, **TPA-PA**, **E-Cz-PA**, and **co-OH-PA**, and hybrid films of **co-OH-PA** with various contents of ZrO_2 (**co-Zr10-PA**, **co-Zr20-PA**, and **co-Zr30-PA**) were successfully prepared. All polyamides exhibit good solubility and thermal stability. As for their EC behaviour, the hybrid films with higher contents of ZrO_2 indeed exhibited lower oxidation potentials compared to **TPA-PA**, further shortening the switching response time. Moreover, a lower R_{ct} value of the hybrid polyamide film could be obtained with increasing the content of ZrO_2. Among all EC films, the **co-Zr20-PA** hybrid film exhibits the most outstanding switching response behaviour (t_c: 2.7 s; t_b:2.0 s). In addition, **ECD-*co*-Zr20-PA** demonstrates highly stable switching reversibility and decreased colouring and bleaching times (t_c: 8.2 s; t_b: 6.9 s) compared to **ECD-TPA-PA**.

Conflicts of interest

The authors declare no competing financial interests.

Acknowledgements

This work was financially supported by the National Science and Technology Council in Taiwan (NSTC 111-2113-M-002-024 and 111-2221-E-002 -028 -MY3). The authors gratefully acknowledge the Instrumentation Center of National Taiwan Normal University (Bruker AV III HD-600) and the Instrumentation Center of National Taiwan University (Orbitrap QE Plus Mass Spectrometry and elementar vario EL cube) for their support and assistance in this work.

References

1 S. H. Hsiao and Y. P. Huang, *Dyes Pigm.*, 2018, **158**, 368–381.
2 M. Thelakkat, *Macromol. Mater. Eng.*, 2002, **287**, 442–461.
3 M. Liang and J. Chen, *Chem. Soc. Rev.*, 2013, **42**, 3453–3488.
4 Z. Ning and H. Tian, *Chem. Commun.*, 2009, **37**, 5483–5495.
5 H. J. Yen and G. S. Liou, *Polym. Chem.*, 2018, **9**, 3001–3018.
6 Z. B. Zhang, M. Fujiki, H. Z. Tang, M. Motonaga and K. Torimitsu, *Macromolecules*, 2002, **35**, 1988–1990.
7 G. Brizius, S. Kroth and U. H. Bunz, *Macromolecules*, 2002, **35**, 5317–5319.
8 J. Bouchard, M. Belletête, G. Durocher and M. Leclerc, *Macromolecules*, 2003, **36**, 4624–4630.
9 S. N. Georgiades and P. G. Nicolaou, *Adv. Heterocycl. Chem.*, 2019, **129**, 1–88.
10 B. Ashton and H. Suschitzky, *J. Chem. Soc.*, 1957, 4559–4562.
11 J. J. J. Li, in *Name Reactions*, Springer, 2014, pp. 68–69.
12 H. J. Knölker, *Chem. Soc. Rev.*, 1999, **28**, 151–157.
13 B. Åkermark, L. Eberson, E. Jonsson and E. Pettersson, *J. Org. Chem.*, 1975, **40**, 1365–1367.
14 F. Bekkar, F. Bettahar, I. Moreno, R. Meghabar, M. Hamadouche, E. Hernáez, J. L. Vilas-Vilela and L. Ruiz-Rubio, *Polymers*, 2020, **12**, 2227.
15 H. M. Wang, S. H. Hsiao, G. S. Liou and C. H. Sun, *J. Polym. Sci., Part A: Polym. Chem.*, 2010, **48**, 4775–4789.
16 S. H. Hsiao, H.-M. Wang, J.-W. Lin, W. Guo, Y.-R. Kung, C.-M. Leu and T.-M. Lee, *Mater. Chem. Phys.*, 2013, **141**, 665–673.
17 S. H. Hsiao, H. M. Wang and S. H. Liao, *Polym. Chem.*, 2014, **5**, 2473–2483.

18 S. H. Hsiao and J. C. Hsueh, *J. Electroanal. Chem.*, 2015, **758**, 100–110.
19 S. H. Hsiao and S. W. Lin, *Polym. Chem.*, 2016, **7**, 198–211.
20 H. J. Knölker, *Chem. Lett.*, 2009, **38**, 8–13.
21 H. J. Knölker and N. O'Sullivan, *Tetrahedron*, 1994, **50**, 10893–10908.
22 H. J. Knölker and W. Fröhner, *J. Chem. Soc., Perkin Trans. 1*, 1998, 173–176.
23 H. J. Yen and G. S. Liou, *Prog. Polym. Sci.*, 2019, **89**, 250–287.
24 B. C. Pan, W. H. Chen, T. M. Lee and G. S. Liou, *J. Mater. Chem. C*, 2018, **6**, 12422–12428.
25 F. W. Li, T. C. Yen and G. S. Liou, *Electrochim. Acta*, 2021, **367**, 137474.
26 Y. W. Chiu, M. H. Pai and G. S. Liou, *ACS Appl. Mater. Interfaces*, 2020, **12**, 35273–35281.
27 J. H. Wu and G. S. Liou, *Adv. Funct. Mater.*, 2014, **24**, 6422–6429.
28 K. H. Park, M. A. Kakimoto and Y. Imai, *J. Polym. Sci., Part A-1: Polym. Chem.*, 1998, **36**, 1987–1994.
29 N. Al Soom and T. Thiemann, *Int. J. Org. Chem.*, 2016, **6**, 1–11.
30 J. F. Ambrose, L. L. Carpenter and R. F. Nelson, *J. Electrochem. Soc.*, 1975, **122**, 876.
31 H. S. Liu, B. C. Pan, D. C. Huang, Y. R. Kung, C. M. Leu and G. S. Liou, *NPG Asia Mater.*, 2017, **9**, e388–e388.
32 H. S. Liu, B. C. Pan and G. S. Liou, *Nanoscale*, 2017, **9**, 2633–2639.